NIH Public Access
Author Manuscript
Nano Lett. Author manuscript; available in PMC 2013 July 11.

Published in final edited form as:
Nano Lett. 2012 July 11; 12(7): 3369–3377. doi:10.1021/nl204175t.

Shape Matters: Intravital Microscopy Reveals Surprising Geometrical Dependence for Nanoparticles in Tumor Models of Extravasation

Bryan Ronain Smith, **Paul Kempen**, **Donna Bouley**, **Alexander Xu**, **Zhuang Liu**, **Nicholas Melosh**, **Hongjie Dai**, **Robert Sinclair**, and **Sanjiv Sam Gambhir**

Abstract

Delivery is one of the most critical obstacles confronting nanoparticle use in cancer diagnosis and therapy. For most oncological applications, nanoparticles must extravasate in order to reach tumor cells and perform their designated task. However, little understanding exists regarding the effect of nanoparticle shape on extravasation. Herein we use real-time intravital microscopic imaging to meticulously examine how two different nanoparticles behave across three different murine tumor models. The study quantitatively demonstrates that high-aspect ratio single-walled carbon nanotubes (SWNTs) display extravasational behavior surprisingly different from, and counterintuitive to, spherical nanoparticles although the nanoparticles have similar surface coatings, area, and charge. This work quantitatively indicates that nanoscale extravasational competence is highly dependent on nanoparticle geometry and is heterogeneous.

Keywords

Single-walled carbon nanotubes; quantum dots; nanoparticle geometry; cancer; intravital microscopy; extravasation

Nanoparticles present numerous revolutionary possibilities for efficient payload delivery to tumors[1]. Dozens of cancer cell biomarkers have been discovered to which nanoparticles can likely be targeted. Yet the tremendous medical impact of these nanoparticles and biomarkers can emerge only if the nanoparticles reach the tumor interstitium where they may interact with the biomarkers that are expressed on the surface of tumor cells. The size of the particle is a well-established factor in its ability to extravasate into tumor interstitium; the effects of particle shape remain unclear. In this study, we employed two commonly used nanoparticles with radically different shape to study the effect of particle geometry in tumor vascular extravasation: spherical quantum dots and high aspect ratio, cylindrical single-walled carbon nanotubes.

The vascular endothelium is a major barrier that impedes the distribution of intravenously injected nanoparticles from access to tumor cells. However, this barrier, and the general transit of nanoparticles from the vessel to the extravascular space, remains largely misunderstood. Understanding this vascular obstacle is critical to elucidating the delivery of nanoparticles to cancer[2,3]. The Enhanced Permeation and Retention (EPR) effect was originally described by Maeda and Matsumura in 1986[4]. It states, in part, that due to the rapid progression of the tumor and its need for nutrients, the blood vessels produced by the tumor are haphazardly formed and thus leaky due to pores between endothelial cells. In many studies it is routinely presumed that nanoparticles will leak across the endothelium, i.e., the EPR effect is assumed to occur for the nanoparticles injected in the study[3,5,6]. Many studies demonstrate that it is often the case that interendothelial pores exist between endothelial cells[3,7], as the nanoparticles in numerous studies reach the tumor cells[3,8,9]. Yet

$watermark-text
$watermark-text
$watermark-text

$watermark-text

$watermark-text

$watermark-text

in other work, it has been shown that relatively small nanoparticles do not extravasate out of the tumor blood vessels[10–12]. It may ultimately be disadvantageous that many in the field now recognize the EPR effect "as a general characteristic of viable and rapidly growing solid tumor[13,14]." This is because the expectation of extravasation could lead to improper choices of nanoparticle as well as study design (which is particularly important for studies designed for translation to humans). This raises critical questions related to nanoparticle delivery: if nanoparticles are to ultimately be successful for diagnostic and therapeutic oncological application, we must understand why some nanoparticles extravasate and others do not in tumor models. We must clarify the dependence of nanoparticle physical parameters (e.g., shape and size) on their delivery through pores in the endothelium. While an agent's size is known to be a major factor in its ability to extravasate in various tumors based on studies of spherical particles[15–18], little to nothing is known about how nanoparticle geometry affects extravasation. Furthermore, prior particle size-extravasation studies focused on larger particles, generally those 100 nm and greater[16–18]. Many of the latest advancements in injectable nanoparticle technologies comprise particles of 1–50 nm in at least one dimension across a wide variety of geometries[19–21]. There is a clear lack of data on how small (1–100 nm) nanoparticle size and especially shape affects extravasation across different tumor types. Bridging this gap in our knowledge through detailed studies in living subjects in combination with high-resolution electron microscopy, as our study addresses, has the potential to help revolutionize nanoparticle design for optimal extravasation.

Little work has been performed in correlating the extravasation of nanoparticles with experimental evidence of the shapes and sizes of the pores in the vasculature. As vascular pores are likely the major route of extravasation[3,5,8,16,17], understanding the relationship between the physical characteristics of the pore in comparison with those of the nanoparticles can yield new insights into extravasation and thus nanoparticle delivery. In this study we examine the extravasation of multiple nanoparticle types in multiple tumor types in living subjects and attempt to connect these observations to the nanoscale morphology of the vasculature via detailed electron microscopic analyses. This link is important as it will ultimately enable us to correlate observable features of the vasculature (such as flow rate, pressure, pore size/shape) with the extravasational behavior of the nanoparticle – this correlation is expected lead to superior choices in nanoparticle properties in research and for clinical translation.

Our study takes advantage of intravital micrsocopy (IVM), which allows detailed microscopic imaging of phenomena in living subjects. IVM applies fluorescence microscopy to image biological events over time. This important technique has enabled researchers to better understand various mechanisms in immunology, neuroscience, and cancer over the past couple decades[22]. Recent work has begun to illustrate the power of IVM to elucidate how nanoparticles target cancer[10,11], and in the present work we apply it to observe and quantify extravasation out of the vasculature in an ear tumor model (Figure 1a). By inoculating different types of tumors in the thin skin of the mouse ear, we used IVM to detect differences in the effective permeability of the blood vessels of the different tumors to two nanoparticle types. We challenged three tumor types (human glioblastoma (brain, U87MG)), ovarian adenocarcinoma (SKOV-3), and colon adenocarcinoma (LS174T) with two commonly-used, but very differently-shaped nanoparticles: quantum dots (qdots) and single-walled carbon nanotubes (SWNTs, Figure 1b).

Qdots and SWNTs display very different physical properties (e.g., shape and size, among others). The approximately spherical crystalline qdots exhibit nearly the same surface area as the high aspect ratio (~100:1), cylindrical SWNTs despite the radical differences in their geometry. Qdots are colloidal semiconductors with excellent photo-stability and other properties valuable for biological applications[23,24]. SWNTs are cylindrical fullerenes with a

$watermark-text

$watermark-text

$watermark-text

set of very unique and often highly useful physical properties for both materials and biological applications. We selected these nanoparticles because (1) their surface area is approximately equal, while their shapes are extremely different and (2) their polyethylene glycol (PEG) surface coatings are similar, which leads to a similar zeta potential distribution. Because the surface coating is similar, we note that it is highly unlikely that one nanoparticle type would be actively transported across the endothelium and the other would not – although they are made of different materials, the exposed surface (i.e., the surface exposed to blood and endothelial cells, and thus likely the only part sensed by the physiology) of the two particles is very similar. Therefore, because the major difference between the two particles is their geometry, we were able to probe the biological barriers and parameters of extravasation with particle shape as the key variable. Furthermore, biologically, SWNTs have a proven, superior ability to enter into tumor sites[25–27], so one major question we sought to answer was whether the unique geometry of SWNTs plays a significant role in their excellent ability to target tumor (10–15% ID/g) by facilitating their transit across endothelial barriers into the tumor interstitium.

During and subsequent to tail-vein injection of 80 pmol of each nanoparticle type, we observed the tumor vasculature using IVM. As previously reported[11,12], qdots did not extravasate in the SKOV-3 tumor model (human ovarian cancer, Figure 2a). Qdots were observed within the tumor vasculature (delineated by the dashed line) within seconds of injection. By one hour after injection, no qdots were visible within the blood vessels, nor in the tumor interstitial regions around the vessel area. Use of smaller qdots (~5 nm) also did not result in extravasation[11]. The blue curves in the Figure 2 graphs represent the entry of nanoparticles into tumor interstitium based on fluorescence intensity (a flat curve with a slope near 0 indicates a lack of extravasation over time). On the other hand, the black curves represent the removal of nanoparticles from circulation, predominantly via reticuloendothelial system uptake (and in some tumor types also due to extravasation). While qdots did not extravasate, even when the high aspect ratio SWNTs (~2–3 nm in the smallest dimension) were injected, they too did not show significant extravasation (Figure 2b). Note that signal observed outside the vasculature in the early SWNT time-point (indicated by red arrows) was due to tissue autofluorescence and not extravasation. As observed by the slopes of the black curves, SWNTs circulate longer (with a half-life greater than twice as long as qdots); therefore, signal can still be observed in the blood vessels after one hour in SWNT-injected animals. We decided to normalize to time (and thus the number of rounds a nanoparticle makes in the mouse circulation) to compare the two nanoparticles, rather than to convolute the question with how circulation times affect their extravasation. However, unlike in the qdot condition in which extravasation was never observed, there was a small degree of extravasational heterogeneity (statistically insignificant, but sporadically a very small amount of extravasation was observed in certain regions) when SWNTs were injected in the SKOV-3 model. The near-total lack of extravasation in SKOV-3 tumors (as also reported by others[12]) across different types and sizes of nanoparticles (but increased extravasation of a small molecule dye in tumor compared with normal vasculature[11]) implies that the pores between endothelial cells in this tumor type are likely very small. It is important to realize that a certain percentage of human tumors may behave this way. This would preclude use of nanoparticles to reach tumor cells by typical techniques, such as the EPR effect (though it may be possible to facilitate uptake of some nanoparticles into tumor interstitium either via use of cells to ferry them in or via transcytotic mechanisms[28,29]). For this reason, in some cases it may be more effective in human disease to target the vasculature with nanoparticles because vascular endothelial targeting is more of a certainty – biomarkers on tumor vascular endothelium are available no matter the pore size and extravasational competence [10,11].

$watermark-text

$watermark-text

$watermark-text

Nevertheless, it remains important in a variety of instances to directly target tumor cells themselves, such as for direct detection or destruction of cancer cells. In most cases, this requires extravasation of the agent. When we examined extravasation of qdots in LS174T tumor (human colon adenocarcinoma)[10], we found that they rapidly and vigorously leaked out of the tumor vessels consistently over 1.5 hours (Figure 3a). Qdots leak from blood vessels and gradually diffuse through tumor interstitium. Yet in contrast to rapid qdot extravasation, when we injected SWNTs into mice bearing LS174T tumors, very little extravasation was observed (Figure 3b). Qdots extravasate much more than SWNTs in LS174T (n=3 per group, 5–8 regions of interest (ROI) per mouse, $p<0.05$, Figures 3a–b and 4). We inferred that the discrepancy might be due to the overall size of SWNTs (200 nm in length, the longest dimension) in comparison with the size of qdots (~20–25 nm in spherical diameter) and the pores of the LS174T tumor blood vessels. For example, if the size of LS174T vascular pores is between 25 nm and 200 nm and they are circular, this explanation might be sterically reasonable depending on the conditions (e.g., shear rates, oncotic/interstitial pressure differences, pore frequency, etc.).

In order to help test our above hypothesis, we subsequently tested a third tumor type. Derived from human glioblastoma, U87MG tumor was challenged with both nanoparticle types. Using IVM, we found that qdots extravasated very little from U87MG vasculature[10] (Figure 3c). Gao et. al. recently published a study on qdots in U87MG tumors in nude mice with histological results that confirm that qdots do not extravasate in this tumor model[30] (it should be noted that the tumor in that study was placed on the mouse shoulder, rather than the ear, which did not appear to have an effect on qdots' extravasational competence). Based on the results from LS174T vasculature, we anticipated that SWNTs also would not likely extravasate. However, surprisingly we found that SWNTs did robustly extravasate from U87MG vasculature. SWNTs extravasated from U87MG vessels significantly more than did qdots (n=3 per group, 5–10 ROIs per mouse, $p<0.05$, Figures 3c–d and 4). This result was unanticipated given that qdots readily extravasated from LS174T vasculature, while SWNTs did not. Note that we did not observe nanoparticle extravasation out of normal vasculature in mice implanted with any of the three tumor types.

Other studies have investigated intravascularly-injected particles across several tumor phenotypes. Jain and colleagues observed the extravasation of spherical liposomes across a number of tumor types[16,17,31] in order to help identify the apparent pore-size cutoffs of the vasculature. Lewis and coworkers characterized the differences in the magnitude of the EPR effect in several tumors using an ^{89}Zr-Albumin particle system. These studies observed how spherical particles behaved in the context of extravasation in various tumor microenvironments. Yet there have been no studies to our knowledge which explore the effect of particle geometry on extravasation. While other work has examined the effect of shape on diffusion in gel matrix as well as reticuloendothelial system uptake[32,33], no investigations on extravasation exist. Previously overlooked, our results indicate that nanoparticle geometry can have a striking and unexpected effect on extravasation and delivery.

Given the remarkable swap in extravasational competence between LS174T and U87MG tumors, we considered a host of potential reasons. The extravasational switch suggested that nanoparticle size alone was not responsible for the difference (size alone could only account for one of the two nanoparticle types extravasating more than the other in all tumor types studied). The surface coating of the nanoparticles was the same (PEG), so surface properties were not expected to be a major factor in the extravasational differences detected (e.g., differential electrostatic repulsion by the pore for one nanoparticle type more than the other). To validate this idea, analysis of the zeta potentials of the nanoparticles revealed similar zeta potential distributions (Supporting Figure 1). We next questioned whether other mechanisms

$watermark-text

$watermark-text

$watermark-text

(than transport across vascular pores) could possibly be implicated, such as active transport; however, we note that the endothelium comprising the tumor is the mouse's and not derived from the tumor cell line. If active transport occurred for example, for SWNTs, it would very likely occur for both tumor types (because the endothelial cells are native to the mouse and should thus be similar in the two tumor types) – the fact that SWNTs extravasated in only one tumor type thus suggests active transport did not occur. Therefore, it is unlikely that endothelial cell active transport would occur for SWNTs (or qdots) in one tumor type but not the other. The most prominent difference between the two particles (their material densities differ only by a factor of 4) is thus their geometry.

Since it is unlikely that the differences in extravasation are due to active transport or other mechanisms, the most likely contributor to the differential extravasation finding is porous endothelium[8,16,17,31]. Hence we asked whether the size and shape of vascular pores found in U87MG and LS174T tumors might help explain the discrepancies observed, in combination with the difference in nanoparticle geometry. Previous careful work estimated the specific pore cutoff sizes for both these (U87MG and LS174T) and other tumors in living subjects[16,17,31]. Yet these estimates were based on spherical particles challenging the endothelium. Therefore, in this context we were obliged to disregard those studies precisely because we are interested in the effects of particle shape (rather than the varied size of spherical particles). We thus decided to directly visualize the pores by conducting a preliminary examination of the vasculature using scanning electron microscopy. We found that pores in the vasculature were fairly rare, which agrees with previous estimates. For instance, pores were found in only 23% of RG-2 glioma microvessels[34]. In our study, we noticed that interendothelial pores in both tumor types tended to be elliptical with an aspect ratio on the order of 2 (Figure 5). Also, we observed that the pores between endothelial cells in LS174T vasculature appeared fairly similar in size and shape to those in U87MG vasculature (though slightly larger in the case of LS174T). In order to test whether the somewhat different size of pores between U87MG and LS174T vasculature could help explain the nanoparticle extravasation properties, we performed a series of well-controlled diffusion experiments *in vitro* to compare the flux of SWNTs and of qdots across 102.9 ± 4.51 nm and 209.2 ± 9.54 nm diameter nanostraw[35] porous membranes (see Supporting Figure 2). We found that SWNTs diffused ~3.5-fold more rapidly than qdots across ~100 nm pores; interestingly, SWNTs and qdots diffused approximately similarly through ~200 nm pores (see Supporting Figures 3–4). The reason these differences were observed likely involves wall effects[36], but is not yet entirely clear. However, these data provide some insights into the differences between SWNT and qdot extravasation in living subjects, as they suggest that slightly smaller U87MG pores may allow significantly more SWNTs to diffuse than qdots, while the slightly increased size of LS174T pores may provide more opportunity for qdots to diffuse. This helps to explain our data. Nevertheless, the result is only helpful in part; the data clearly suggest that other factors must also be partially responsible for the extravasational differences observed.

One factor that may also help explain the difference in extravasation is that U87MG tumors display fenestrated endothelium[38] – the "holes" are ~5.5 nm and fairly common (these fenestrae are different from the interendothelial pores discussed above). While the U87MG "pore cutoff size" by spherical particle challenge was determined to be lowest of all tumors tested across several studies, the overall permeability to albumin was highest[31]; this indicates that there may be many very small pores through which SWNTs could traverse via Brownian (diffusive) motion, but through which qdots sterically could not. This thus may be another reason why there is a huge difference between U87MG and LS174T tumors (in qdot/SWNT extravasation). It is because qdots would be physically unable to exit the vasculature through fenestrations, while in one dimension, SWNTs could diffuse into the interstitium via Brownian motion (given the presence of many fenestrae, SWNTs may

$watermark-text

$watermark-text

$watermark-text

diffuse much more in U87MG tumors due to the fenestrations and slower flow, see Supporting Information).

The nanoparticles and the endothelial pores in this work are subject to physical, quantifiable forces which should be subject to computational analysis. The development of computational simulations for nanoparticle delivery is rapidly emerging and is critical to propel the field forward. Yet despite its promise, current models and analyses can not explain our observations. Only by fully and realistically simulating the complex interactions between the hydrodynamic flow forces, nanoparticle shape and size, Brownian forces, margination properties, and vascular pore size and shape can we expect to elucidate the differential extravasation properties observed. We are working to establish such mathematical simulations; we have also developed a preliminary qualitative hypothesis to explain our data given the local hydrodynamic and oncotic pressure forces specific to each tumor type (see Supporting Information).

Our extravasation results were obtained in nude mice in an ear tumor xenograft model, and it is necessary to appreciate that these results may not be the same when the nanoparticles are assessed in other mouse strains, tumor models, or even other sites of tumor within a mouse. However, it is critical to understand that the specific models we used are not important; rather, the essential point is that given a set of tumor conditions (represented by U87MG and LS174T in the ear, with their specific physical properties such as pore size/shape and flow conditions) and two nanoparticles (with similar charge, surface coating, and density), nanoparticle geometry significantly affects the ability to leak from vessels and thus the ability of the agent to reach tumor cells. In particular, not only is the effect substantial, but *the data imply that a particular particle geometry will not always be "better" to maximize extravasation* – i.e., there appears to be an acute dependence on other properties, such as vascular flow and pressure conditions, etc. This represents a departure from the current paradigm that only size matters (with acknowledgment that shape (and charge) could possibly also impact extravasation, as we establish here). This potential shift in perspective should lead to greater, more informed consideration in the choice of particle geometry when selecting a particle for tumor targeting in pre-clinical and ultimately clinical situations.

A review of the literature confirms that it is commonly assumed that nanoparticles extravasate from tumor blood vessels via the EPR effect[7,13]. Yet in our study we found that across six conditions (comprising three different, commonly used tumor models, each challenged with two nanoparticle types), only two to three conditions exhibited significant extravasation (Figure 4a) – i.e., more often than not, nanoparticles were not truly reaching tumor cells. Not only does heterogeneity exist across tumor types, but recently extravasation was also shown to be dependent on tumor stage[39]. Such low and unpredictable rates of extravasational competence underscore the great value in better elucidating the mechanisms of extravasation in order to rationally design nanoparticles for optimal extravasation. Enabling a greater number of nanoparticles to reach the tumor interstitium and interact with tumor cells is a key element in creating successful molecular imaging and therapeutic agents. Yet the common presumption that extravasation occurs, and is producing the effect observed (e.g., diagnostic signal or a therapy) in many nanoparticle-based imaging[7,25,27,40] and therapeutic[41] tumor studies, may ultimately diminish the utility of nanoparticles in oncology. Understanding the factors involved in a nanoparticle's success in reaching the tumor bed is thus vital to nanoparticle technologies reaching the clinic.

In conclusion, we have found that there are large differences in the extravasation of two nanoparticle varieties across three tumor types. Both nanoparticles essentially do not extravasate in SKOV-3 tumors. Yet the dynamics of extravasation were highly complex in LS174T and U87MG tumors. Intriguingly, IVM demonstrated that qdots extravasate more

$watermark-text

$watermark-text

$watermark-text

than SWNTs in LS174T, while SWNTs extravasate much more than qdots in U87MG tumors as represented by the schematic in Figure 4b. Nanoparticle geometry therefore appears to play a complex and potentially major role in extravasation in tumors. While nanoparticle diffusion experiments across synthetic pores partially explain the results, more complete understanding of this multifaceted effect will be important in order to design optimal, efficient tumor-targeting nanoparticles to advance into the clinic. Indeed, knowing the physical parameters of a patient's tumor should prove essential to providing personalized oncological care, as a specific particle geometry (and size) could be designed for the appropriate tumor conditions.

Methods

Nanoparticles

Dye-labeled peptide-conjugated SWNT bioconjugates were prepared as previously reported[26,42] with slight modifications as follows. Raw Hipco SWNTs were sonicated in an aqueous solution of DSPE-PEG_{5000}-Amine (NOF Corp) for 1 h and centrifuged at 24,000 g for 6 h to obtain short, PEGylated SWNTs in supernatant. Filtration through 100 kDa filters (Millipore) was used to remove excess coating polymer. To conjugate Cy5.5 dye, Cy5.5-NHS (Invitrogen) and sulfo-SMCC (sulfosuccinimidyl 4-N-maleimidomethyl cyclohexane-1-carboxylate) (Pierce) were subsequently mixed at 1:5 molar ratios (0.2mM : 1mM) and incubated with PEGylated SWNTs for 2 hours at pH 7.4. Excess dye was removed via filtration.

SWNT concentrations were determined spectrophotometrically (using a DU 640 from Beckman Coulter, Fullerton, CA) with an extinction coefficient of 3.1×10^6 1/mol*cm at 808 nm as described previously. They were further analyzed for Cy5.5 content (~20 Cy5.5 per SWNT).

Near-infrared emitting PEGylated quantum dots with amino functionalization were obtained from Invitrogen (Amino Qdots 800, Carlsbad, CA). Qdot experiments were performed by exchanging the solute into PBS and proceeding without further modification. Qdot concentration was established via spectrophotometry using a DU640 (Beckman Coulter, Fullerton, CA) with extinction coefficient of 3.1×10^6 mol^{-1} cm^{-1} at 488 nm. Qdots were characterized also with dynamic light scattering (ZetaPlus Analyzer, Brookhaven Instruments Corporation, Holtsville, NY) for hydrodynamic radius and presence of aggregates. The surface charge of both qdots and SWNTs were analyzed using a ZetaSizer Nano ZS (Malvern Instruments, Worcestershire, UK).

Tumor model

To image the tumor microenvironment, stable, bright green cell lines were produced. Human glioblastoma cells (U87MG), human colon adenocarcinoma cells (LS174T), and human ovarian carcinoma cells (SKOV3) (all obtained from American Type Culture Collection, ATCC) were labeled with enhanced green fluorescent protein (EGFP). The stable EGFP expressing cell lines were established using a lentiviral vector (pRRLsin18.CMV-EGFP, a gift from Luigi Naldini, HSR-TIGET, Italy) with an EGFP transgene. These cells were incubated overnight in media containing high titer virus, then cells with very high EGFP expression were sorted using FACS. Cells were grown in ATCC-recommended medium. Nude female mice (nu/nu, Charles River, Wilmington, MA) were inoculated with 200,000–300,000 U87MG, LS174T, or SKOV-3 cells in the ear in very low volume by pulling up the skin, sliding in the needle several mm, and injecting. Tumors were imaged ~7–10 days after inoculation, at which point they were ~5–7 mm in diameter. All animal procedures were approved by the Stanford University Institutional Animal Care and Use Committee.

$watermark-text

$watermark-text

$watermark-text

Intravital Microscopy

Nude mice (N=18) were used for this study across the 6 groups. Mice were anesthetized with isoflurane and the ear of interest was positioned beneath the objective of the IV-100 intravital microscope (Olympus, Center Valley, PA) and stabilized. Long-circulating dye Angiosense 680 or Angiosense 750 (VisEn Medical, Woburn, MA) was injected to outline the vasculature. Approximately 80 pmol of either qdots or SWNTs in 200 μl PBS was subsequently injected. Mice were imaged during injection and until the nanoparticles were no longer visible in the vasculature (generally up to ~3–4 hours). Mice were imaged using the 488, 633, and 748 nm laser lines, and three appropriate output channels (green, red, and near-infrared filter sets). Output channels were scanned sequentially to prevent filter bleed-through. Extravasation was analyzed by reference to the presence of nanoparticles outside Angiosense-marked blood vessels.

Data were analyzed by using a region-of-interest (ROI) analysis. Z-stacks were generated by optically sectioning through the ROI (typically 10–20 sections per region) at every time-point. For each mouse, at early and late time-points in the same field-of-view (FOV), 4–8 regions-of-interest (ROIs) were placed outside of blood vessels. The same number of ROIs were placed within blood vessels to assess changes in fluorescence within the vasculature. The fluorescence intensity was evaluated over time in each ROI and an average value across all ROIs was obtained at each time-point. From this, a parameter – change in fluorescence intensity per unit time – was calculated. This parameter was obtained for each mouse in the group, we averaged across all the mice, and then computed standard errors of the mean. Percent fluorescence intensity per unit time was also computed.

Electron Microscopy

For scanning electron microscopy, we fixed tissues via modifications of the protocol of Hashizume et. al[8]. Briefly, the tissues were fixed by vascular perfusion of a solution consisting of 0.5% glutaraldehyde and 1% paraformaldehyde in buffer (0.075 mol/L sodium cacodylate buffer, pH 7.4) in nude mice with ear tumors of 6–10 mm. The tumors were removed, immersed in 2.5% glutaraldehyde in the cacodylate buffer for about 2 hours, then subsequently embedded in 10% agarose. The blood vessel luminal surface in tumors was exposed by use of a microtome to cut sections 8 μm in thickness. The sections were subsequently rinsed using cacodylate buffer, then immersed in cacodylate buffered 2% tannic acid for 24 hours, rinsed, and finally immersed in 2% OsO4 in 0.1 mol/L cacodylate buffer for 2 hours at 4°C. Following dehydration of the sections with ethanol, they were permeated with 100% *t*-butanol and freeze-dried under vacuum. Histology slides of fixed tumor tissue stained with hematoxylin and eosin and without cover slips were imaged using a Leica DM 2000 light microscope. Images were taken and stitched together to create a large composite image of the tissue. The histology slides were then coated with a thin AuPd film to improve conductivity and imaged in the scanning electron microscope. A Magellan XHR SEM operated at 5 kV with a probe current of 50 pA was utilized to collect secondary electron images of the tissue samples. The light microscopy histology images were utilized to locate blood vessels within the tissue sections which were then imaged in the SEM to locate defects within these vessels. The presence of remaining red blood cells was used to indicate the presence of a blood vessel.

Statistics

For each tumor type, the change in fluorescence intensity per unit time for all mice in the group using qdots was compared against the values when employing SWNTs. A two-tailed t-test was used to make the comparison and $p<0.05$ was taken to be significant.

$watermark-text

$watermark-text

$watermark-text

Supplementary Material

Refer to Web version on PubMed Central for supplementary material.

Acknowledgments

This study was supported in part by the following grants: NCI U54 CA119367 (SSG) and NCI ICMIC P50 CA114747 (SSG). BRS was supported by an NIH R25T postdoctoral training grant and currently by a K99/R00 Award (NCI K99 CA160764). We gratefully acknowledge the assistance of John Perrino and Lydia Joubert of the Cell Sciences Imaging Facility in the Beckman Center for technical assistance, Jim Strommer for graphics assistance, and Christine Wang for her critical reading of the manuscript.

References

1. Peer D, Karp JM, Hong S, Farokhzad OC, Margalit R, Langer R. Nanocarriers as an emerging platform for cancer therapy. Nat Nanotechnol. 2007; 2:751–760. [PubMed: 18654426]
2. Danhier F, Feron O, Preat V. To exploit the tumor microenvironment: Passive and active tumor targeting of nanocarriers for anti-cancer drug delivery. J Control Release. 2010; 148:135–146. [PubMed: 20797419]
3. Jain RK, Stylianopoulos T. Delivering nanomedicine to solid tumors. Nat Rev Clin Oncol. 2010; 7:653–664. [PubMed: 20838415]
4. Matsumura Y, Maeda H. A new concept for macromolecular therapeutics in cancer chemotherapy: mechanism of tumoritropic accumulation of proteins and the antitumor agent smancs. Cancer Res. 1986; 46:6387–6392. [PubMed: 2946403]
5. McDonald DM, Baluk P. Significance of blood vessel leakiness in cancer. Cancer Res. 2002; 62:5381–5385. [PubMed: 12235011]
6. Fukumura D, Jain RK. Tumor microvasculature and microenvironment: targets for anti-angiogenesis and normalization. Microvasc Res. 2007; 74:72–84. [PubMed: 17560615]
7. Medarova Z, Pham W, Farrar C, Petkova V, Moore A. In vivo imaging of siRNA delivery and silencing in tumors. Nat Med. 2007; 13:372–377. [PubMed: 17322898]
8. Hashizume H, Baluk P, Morikawa S, et al. Openings between defective endothelial cells explain tumor vessel leakiness. Am J Pathol. 2000; 156:1363–1380. [PubMed: 10751361]
9. Sarin H, Kanevsky AS, Wu H, et al. Physiologic upper limit of pore size in the blood-tumor barrier of malignant solid tumors. J Transl Med. 2009; 7:51. [PubMed: 19549317]
10. Smith BR, Cheng Z, De A, Rosenberg J, Gambhir SS. Dynamic visualization of RGD-quantum dot binding to tumor neovasculature and extravasation in multiple living mouse models using intravital microscopy. Small. 2010; 6:2222–2229. [PubMed: 20862677]
11. Smith BR, Cheng Z, De A, Koh AL, Sinclair R, Gambhir SS. Real-time intravital imaging of RGD-quantum dot binding to luminal endothelium in mouse tumor neovasculature. Nano Lett. 2008; 8:2599–2606. [PubMed: 18386933]
12. Kong G, Braun RD, Dewhirst MW. Hyperthermia enables tumor-specific nanoparticle delivery: effect of particle size. Cancer Res. 2000; 60:4440–4405. [PubMed: 10969790]
13. Maeda H, Sawa T, Konno T. Mechanism of tumor-targeted delivery of macromolecular drugs, including the EPR effect in solid tumor and clinical overview of the prototype polymeric drug SMANCS. J Control Release. 2001; 74:47–61. [PubMed: 11489482]
14. Maeda H, Wu J, Sawa T, Matsumura Y, Hori K. Tumor vascular permeability and the EPR effect in macromolecular therapeutics: a review. J Control Release. 2000; 65:271–284. [PubMed: 10699287]
15. Perrault SD, Walkey C, Jennings T, Fischer HC, Chan WC. Mediating tumor targeting efficiency of nanoparticles through design. Nano Lett. 2009; 9:1909–1915. [PubMed: 19344179]
16. Yuan F, Dellian M, Fukumura D, et al. Vascular permeability in a human tumor xenograft: molecular size dependence and cutoff size. Cancer Res. 1995; 55:3752–3756. [PubMed: 7641188]
17. Yuan F, Leunig M, Huang SK, Berk DA, Papahadjopoulos D, Jain RK. Microvascular permeability and interstitial penetration of sterically stabilized (stealth) liposomes in a human tumor xenograft. Cancer Res. 1994; 54:3352–3356. [PubMed: 8012948]

$watermark-text
$watermark-text
$watermark-text

18. Stroh M, Zimmer JP, Duda DG, et al. Quantum dots spectrally distinguish multiple species within the tumor milieu in vivo. Nat Med. 2005; 11:678–682. [PubMed: 15880117]
19. Simone EA, Dziubla TD, Muzykantov VR. Polymeric carriers: role of geometry in drug delivery. Expert Opin Drug Deliv. 2008; 5:1283–1300. [PubMed: 19040392]
20. Merkel TJ, Herlihy KP, Nunes J, Orgel RM, Rolland JP, DeSimone JM. Scalable, shape-specific, top-down fabrication methods for the synthesis of engineered colloidal particles. Langmuir. 2010; 26:13086–13096. [PubMed: 20000620]
21. Kim BY, Rutka JT, Chan WC. Nanomedicine. N Engl J Med. 2010; 363:2434–2443. [PubMed: 21158659]
22. Weigert R, Sramkova M, Parente L, Amornphimoltham P, Masedunskas A. Intravital microscopy: a novel tool to study cell biology in living animals. Histochem Cell Biol. 2010; 133:481–491. [PubMed: 20372919]
23. Michalet X, Pinaud FF, Bentolila LA, et al. Quantum dots for live cells, in vivo imaging, and diagnostics. Science. 2005; 307:538–544. [PubMed: 15681376]
24. Zrazhevskiy P, Gao X. Multifunctional Quantum Dots for Personalized Medicine. Nano Today. 2009; 4:414–428. [PubMed: 20161004]
25. De la Zerda A, Zavaleta C, Keren S, et al. Carbon nanotubes as photoacoustic molecular imaging agents in living mice. Nat Nanotechnol. 2008; 3:557–562. [PubMed: 18772918]
26. Liu Z, Cai W, He L, et al. In vivo biodistribution and highly efficient tumour targeting of carbon nanotubes in mice. Nat Nanotechnol. 2007; 2:47–52. [PubMed: 18654207]
27. Zavaleta C, de la Zerda A, Liu Z, et al. Noninvasive Raman spectroscopy in living mice for evaluation of tumor targeting with carbon nanotubes. Nano Lett. 2008; 8:2800–2805. [PubMed: 18683988]
28. Leimgruber A, Berger C, Cortez-Retamozo V, et al. Behavior of endogenous tumor-associated macrophages assessed in vivo using a functionalized nanoparticle. Neoplasia. 2009; 11:459–468. 2 p following 68. [PubMed: 19412430]
29. Sugahara KN, Teesalu T, Karmali PP, et al. Coadministration of a tumor-penetrating peptide enhances the efficacy of cancer drugs. Science. 2010; 328:1031–1035. [PubMed: 20378772]
30. Gao J, Chen K, Xie R, et al. In vivo tumor-targeted fluorescence imaging using near-infrared non-cadmium quantum dots. Bioconjug Chem. 2010; 21:604–609. [PubMed: 20369817]
31. Hobbs SK, Monsky WL, Yuan F, et al. Regulation of transport pathways in tumor vessels: role of tumor type and microenvironment. Proceedings of the National Academy of Sciences of the United States of America. 1998; 95:4607–4612. [PubMed: 9539785]
32. Decuzzi P, Godin B, Tanaka T, et al. Size and shape effects in the biodistribution of intravascularly injected particles. Journal of controlled release : official journal of the Controlled Release Society. 2010; 141:320–327. [PubMed: 19874859]
33. Pluen A, Netti PA, Jain RK, Berk DA. Diffusion of macromolecules in agarose gels: comparison of linear and globular configurations. Biophysical journal. 1999; 77:542–552. [PubMed: 10388779]
34. Schlageter KE, Molnar P, Lapin GD, Groothuis DR. Microvessel organization and structure in experimental brain tumors: microvessel populations with distinctive structural and functional properties. Microvascular research. 1999; 58:312–328. [PubMed: 10527772]
35. Vandersarl JJ, Xu AM, Melosh NA. Nanostraws for Direct Fluidic Intracellular Access. Nano letters. 2011; 12(8):3881–3886. [PubMed: 22166016]
36. Jones RB. Diffusion of polymers near a fluid-fluid interface or a wall. Physica A: Statistical Mechanics and its Applications. 1975; 83:72–84.
37. Schmidt MM, Wittrup KD. A modeling analysis of the effects of molecular size and binding affinity on tumor targeting. Mol Cancer Ther. 2009; 8:2861–2871. [PubMed: 19825804]
38. Pen A, Moreno MJ, Durocher Y, Deb-Rinker P, Stanimirovic DB. Glioblastoma-secreted factors induce IGFBP7 and angiogenesis by modulating Smad-2-dependent TGF-beta signaling. Oncogene. 2008; 27:6834–6844. [PubMed: 18711401]
39. Hori K, Nishihara M, Yokoyama M. Vital microscopic analysis of polymeric micelle extravasation from tumor vessels: macromolecular delivery according to tumor vascular growth stage. J Pharm Sci. 2010; 99:549–562. [PubMed: 19544373]

40. Cai W, Shin DW, Chen K, et al. Peptide-labeled near-infrared quantum dots for imaging tumor vasculature in living subjects. Nano Lett. 2006; 6:669–676. [PubMed: 16608262]
41. Davis ME, Chen ZG, Shin DM. Nanoparticle therapeutics: an emerging treatment modality for cancer. Nat Rev Drug Discov. 2008; 7:771–782. [PubMed: 18758474]
42. Liu Z, Tabakman SM, Chen Z, Dai H. Preparation of carbon nanotube bioconjugates for biomedical applications. Nat Protoc. 2009; 4:1372–1382. [PubMed: 19730421]

$watermark-text
$watermark-text
$watermark-text

$watermark-text
$watermark-text
$watermark-text

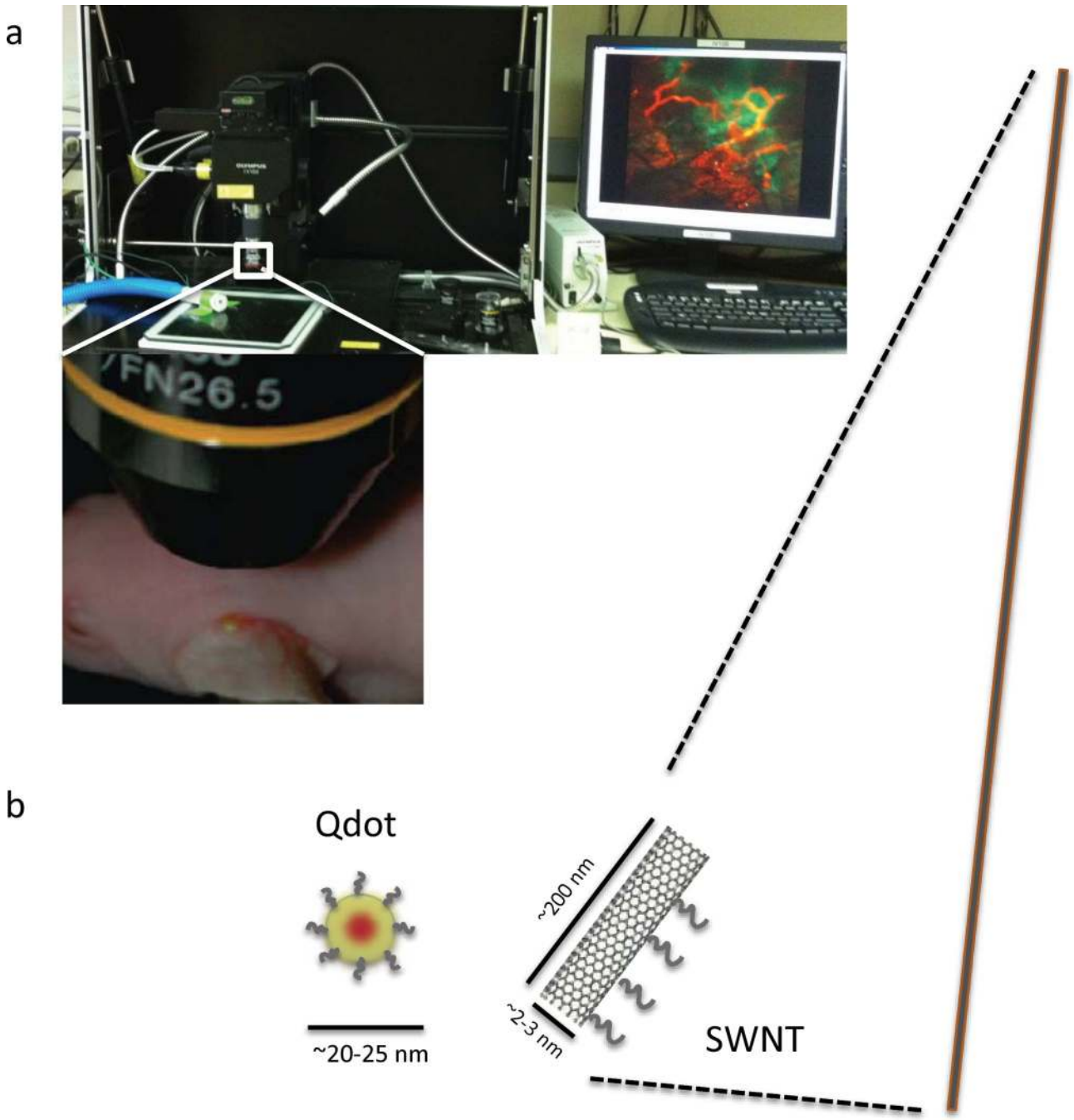

Figure 1.
Experimental set-up. (a) Our intravital microscope set-up is shown, with an image of an ear tumor of an anesthetized mouse being imaged. (b) The two nanoparticles we employ in this work are illustrated as cartoons. The quantum dot is approximately spherical and has a hydrodynamic diameter of ~20 nm. High aspect ratio single-walled carbon nanotubes are ~2–3 nm in diameter and ~200 nm in length. The quantum dot on the left and the nanotube cartoon on the far right extending across the height of the figure are drawn to scale with respect to one another. The clear differences in size and scale are more easily grasped by visualization with this graphic.

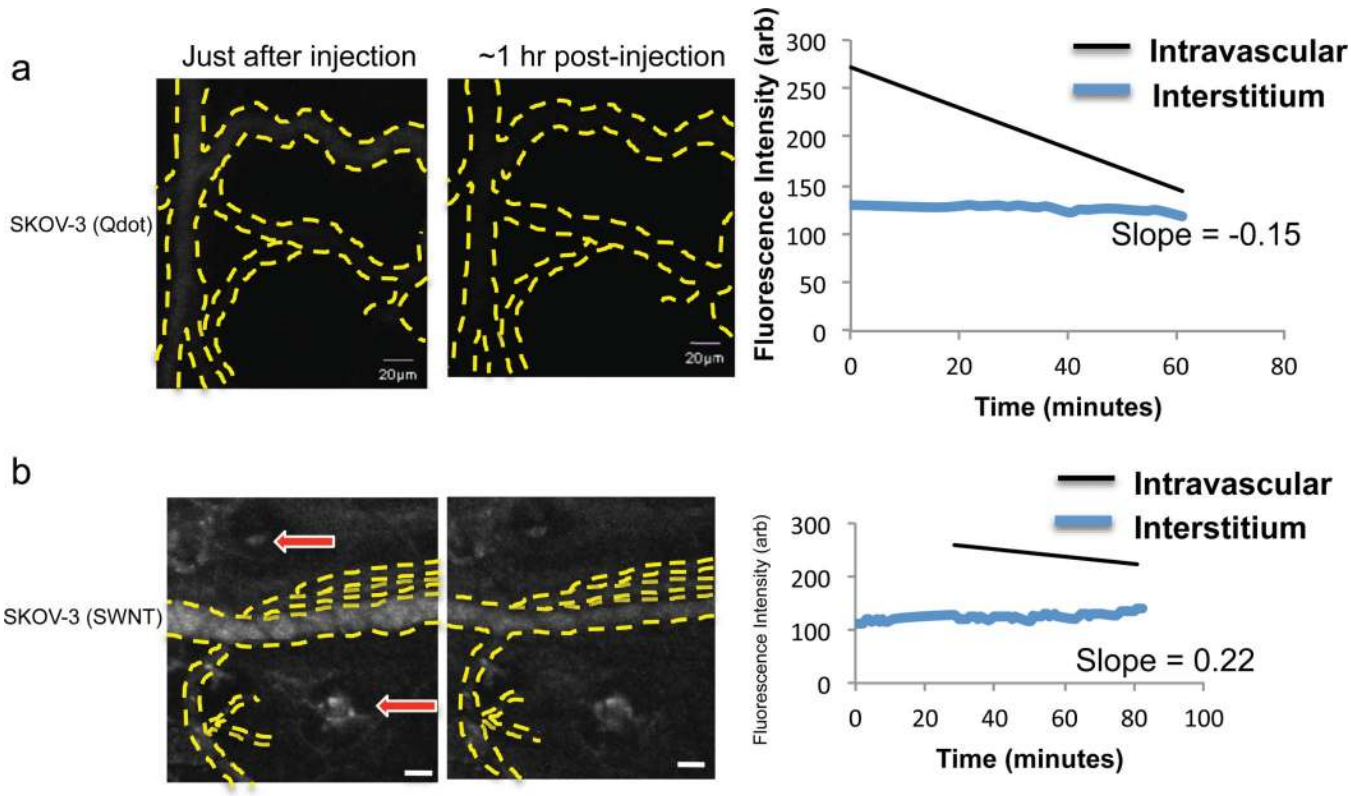

Figure 2.

SKOV-3 tumor extravasation of qdots and SWNTs. Images on the left display nanoparticles (grayscale) within blood vessels in SKOV-3 tumor within minutes of nanoparticle injection (the tumor channel was removed for ease of viewing the vasculature). The location of vessels is specified by the dashed lines. Each set of images is accompanied by a graph on the right of the change in fluorescence intensity over time, in both the extravascular space (i.e., extravasated nanoparticles, illustrated by the blue curve) and nanoparticles in the intravascular space (illustrated by the black curve). The estimated slope (assuming a linear fit) is indicated for the extravasation curves to provide an approximate, quantitative appreciation for the rate of nanoparticle leakage. (a) Qdots (gray) can be easily observed in the blood vessels soon after injection. By one hour postinjection, no qdots are visible in the vessels nor outside the vessels, in the tumor interstitium. Scale bars represent 20 μm. (b) SWNTs (gray) are visible minutes after injection. The arrows point to hair follicles which are autofluorescent in their center; furthermore, general autofluorescence pervades the image. However, it is clear that by one hour post-injection, the fluorescence has not increased. This is quantified in graphs. Scale bars represent 50 μm.

$watermark-text
$watermark-text
$watermark-text

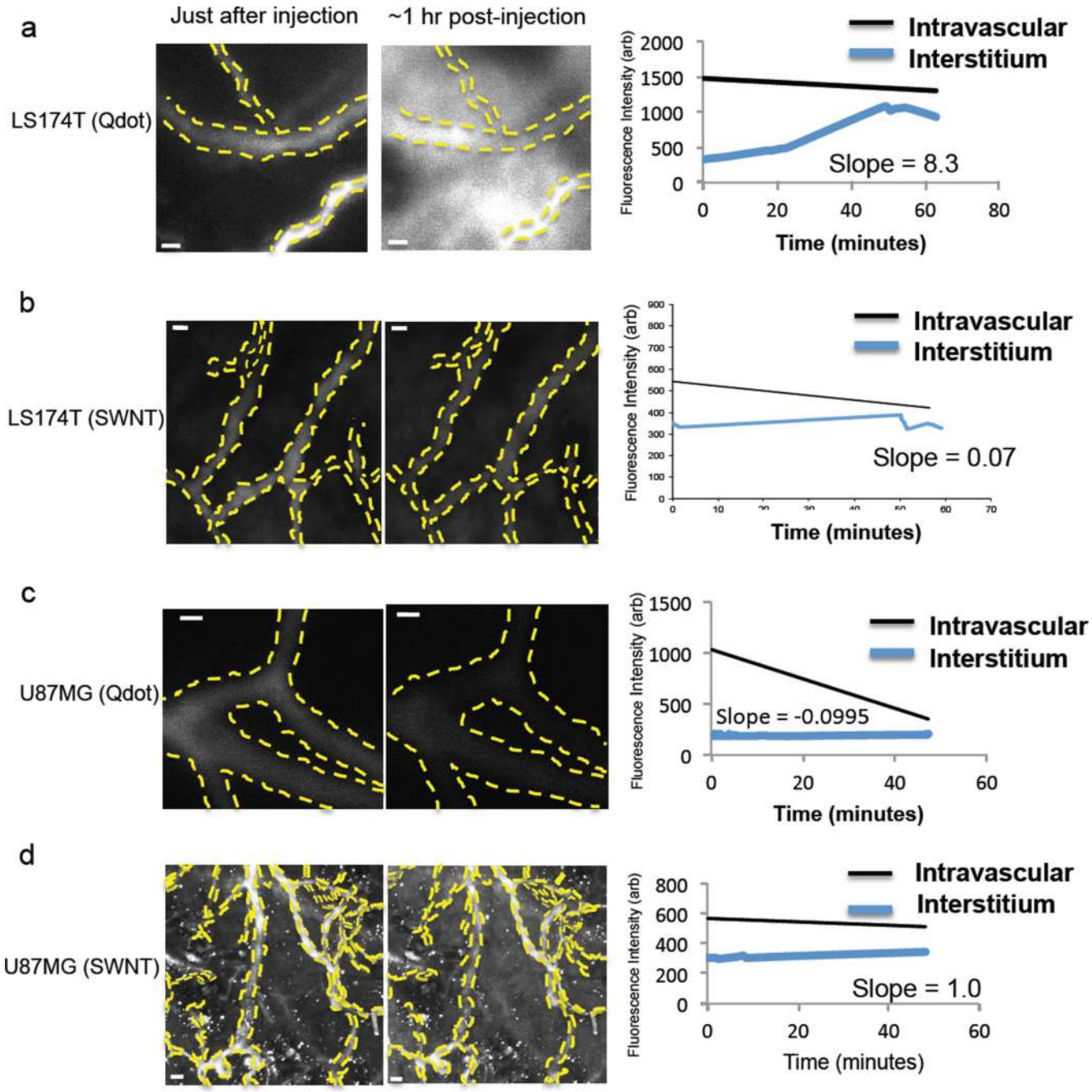

Figure 3.

LS174T and U87MG tumor extravasation of qdots and SWNTs. As in Figure 2, blood vessels are represented by dashed lines and nanoparticles are in grayscale. Each set of images is accompanied by a fluorescence intensity graph on the right, for extravasated nanoparticles (blue curve) and nanoparticles still circulating within the blood vessels (black curve). The estimated slope (assuming a linear fit) is indicated for the extravasation curves to provide an approximate, quantitative appreciation for the rate of nanoparticle leakage. (a) Qdots (grayscale) in LS174T tumor extravasate robustly out of the blood vessels within one hour of injection (see graph for the rapidity and monotonic increase over 50 minutes). It is notable that the very high signal produced by extravasated qdots in this image (due to the

$watermark-text
$watermark-text
$watermark-text

high level of extravasation) somewhat convolutes measurements of fluorescence intensity within the blood vessels, explaining the low absolute value of the slope in the black (intravascular) curve on the right. (b) On the other hand, SWNTs do not extravasate nearly as much as qdots. Note that they do extravasate minimally (by reference to the minor signal increase in the interstitium outside the vasculature between the two time-points). All scale bars in (a) and (b) represent 20 μm. (c) Qdots in U87MG tumor do not extravasate out of the vasculature, as can be observed in the tumor interstitium outside the blood vessels since there is no apparent change in fluorescence intensity. The graph shows this quantitatively. Scale bar represents 10 μm. (d) In the images in the SWNT condition, autofluorescence is visible in the condition immediately after injection (both diffuse autofluorescence as well as intense, punctate autofluorescence). Unexpectedly, as observed by the clear increase in extravascular intensity, SWNTs extravasate in U87MG tumors. This is supported by the graph quantifying the fluorescence increase. Scale bar is 50 μm.

$watermark-text
$watermark-text
$watermark-text

$watermark-text
$watermark-text
$watermark-text

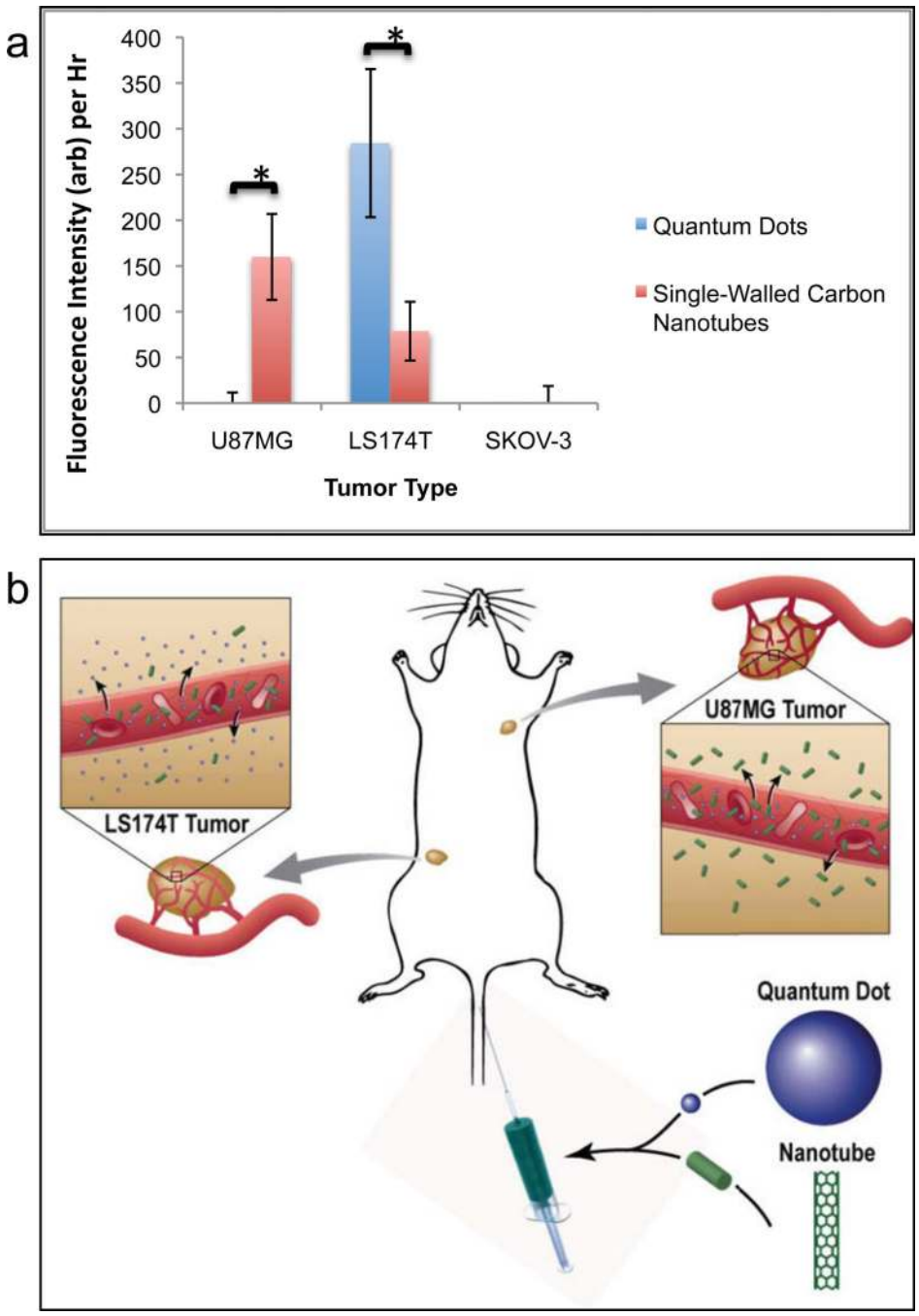

Figure 4.

The extravasation of qdots and SWNTS from the vasculature of murine tumor models. (a) The extravasation (averaged over all mice per nanoparticle/tumor group) of qdots is compared with that of SWNTs for each tumor type. There is a significant difference between the extravasation of the two nanoparticle types for U87MG tumors. The extravasation difference is also significant for LS174T tumors, but surprisingly the nanoparticle types are reversed in terms of their extravasational competence compared with U87MG tumors. Note that qdots displayed nearly zero average extravasation for both U87MG and SKOV-3 tumors, as did SWNTs in the SKOV-3 condition. Note also that SWNTs do appear to extravasate from LS174T, though qdots extravasate much better. * Denotes significance,

with $p<0.05$. (b) Overview depiction of nanoparticle extravasation. The schematic shows that qdots extravasate from LS174T tumor but not U87MG tumor, while SWNTs extravasate from U87MG tumors but only minimally from LS174T.

$watermark-text
$watermark-text
$watermark-text

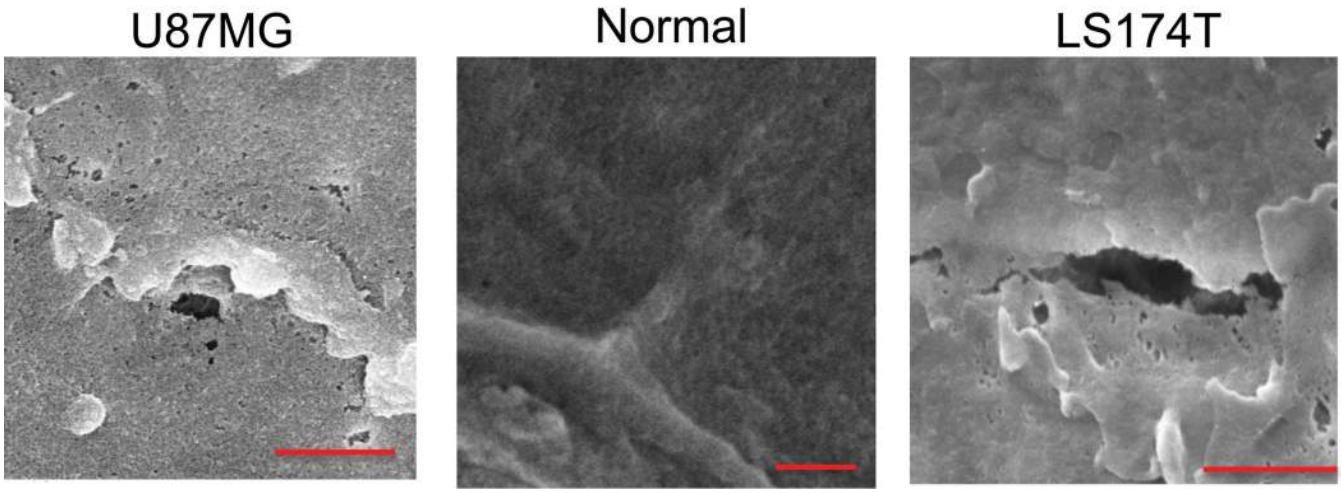

Figure 5.
Scanning Emission Microscopy on Tumor and Normal Blood Vessels. SEM images show pores in U87MG and LS174T tumor vasculature on the apparent boundary between endothelial cells. Pores are not observed on the boundary in the vasculature of a mouse ear without tumor. Scale bars: U87MG (500nm), Normal (1 μm), and LS174T (1 μm).

$watermark-text
$watermark-text
$watermark-text